

Article

H₂O₂ Induces Calcium and ERMES Complex-Dependent Mitochondrial Constriction and Division as Well as Mitochondrial Outer Membrane Remodeling in *Aspergillus nidulans*

Verónica Garrido-Bazán  and Jesús Aguirre * 

Departamento de Biología Celular y del Desarrollo, Instituto de Fisiología Celular, Universidad Nacional Autónoma de México, Apartado Postal 70-242, Ciudad de México 04510, Mexico

* Correspondence: jaguirre@ifc.unam.mx

Abstract: The dynamin-like protein DnmA and its receptor FisA are essential for H₂O₂-induced mitochondrial division in *Aspergillus nidulans*. Here, we show that in the absence of DnmA or FisA, mitochondria show few spontaneous transient constrictions, the frequency of which is extensively increased by H₂O₂ or the carbonyl cyanide m-chlorophenyl hydrazone (CCCP). While H₂O₂-induced constrictions are transient, CCCP induces a drastic and irreversible alteration of mitochondrial filaments. H₂O₂ induces a gradual mitochondrial depolarization, while CCCP-induced depolarization is abrupt. The calcium chelator BAPTA-AM prevents the formation of mitochondrial constrictions induced by either H₂O₂ or CCCP. H₂O₂ also induces major rearrangements of the mitochondrial outer membrane, which remain after constrictions dissipate, as well as changes in endoplasmic reticulum (ER) and nuclear morphology. Similar mitochondrial constriction, ER and nuclear morphology changes are detected during the early stages of asexual development. ER and ER-Mitochondria encounter structure (ERMES) complex—composed of proteins Mdm10, Mmm1, Mdm43 and Mdm12—are important for mitochondrial division in *Saccharomyces cerevisiae*. As the Mdm10 ortholog MdmB was found to be essential in *A. nidulans*, we evaluated its functions in $\Delta m d m B$ terminal mutants and $\Delta m d m B$ heterokaryons. $\Delta m d m B$ conidia produce a short germ tube that fails to grow further, in which inherited mitochondria become gigantic and round shaped, lacking clear contacts with the ER. In slow-growing $\Delta m d m B$ heterokaryotic mycelia, multiple hyphae contain very long mitochondria with high ROS levels, as occur in $\Delta d n m A$ and $\Delta f i s A$ mutants. In this hyphae, H₂O₂ fails to induce mitochondrial constrictions but not outer mitochondrial membrane reshaping, indicating that these are two separate effects of H₂O₂. Our results indicate that H₂O₂ induces a generalized mitochondrial constriction response, prior to actual division, involving gradual depolarization; they also indicate that Ca²⁺ and the ERMES complex are critical for both mitochondrial constriction and division. This supports a view of mitochondrial dynamics as the result of a cascade of signaling events that can be initiated in vivo by H₂O₂.

Keywords: ROS signaling; mitochondrial dynamics; mitochondrial fission; endoplasmic reticulum; Drp1; ERMES; calcium



Citation: Garrido-Bazán, V.; Aguirre, J. H₂O₂ Induces Calcium and ERMES Complex-Dependent Mitochondrial Constriction and Division as Well as Mitochondrial Outer Membrane Remodeling in *Aspergillus nidulans*. *J. Fungi* **2022**, *8*, 829. <https://doi.org/10.3390/jof8080829>

Academic Editor: Ulrich Kück

Received: 1 July 2022

Accepted: 1 August 2022

Published: 9 August 2022

Publisher's Note: MDPI stays neutral with regard to jurisdictional claims in published maps and institutional affiliations.



Copyright: © 2022 by the authors. Licensee MDPI, Basel, Switzerland. This article is an open access article distributed under the terms and conditions of the Creative Commons Attribution (CC BY) license (<https://creativecommons.org/licenses/by/4.0/>).

1. Introduction

We are interested in understanding the roles of reactive oxygen species (ROS) as physiological regulatory signals [1,2]. ROS play critical roles in cell differentiation in fungi, where ROS-producing NADPH oxidases are essential for sexual differentiation [3–7]. Consistent with this, mutants affected in components of the antioxidant response show premature sexual differentiation and decreased asexual development [8,9].

H₂O₂ is considered to be the most relevant ROS in redox biology [10]. Indeed, in the fungus *Aspergillus nidulans*, H₂O₂ activates the MAPKs Saka, MpkC [8,11,12], MpkA and

MpkB [13], and changes the phosphorylation patterns of multiple other proteins involved in signal transduction, gene expression, metabolism and development [13]. SakA mediates the nuclear localization of its substrate SrkA, and when SakA is not present, H₂O₂ induces SrkA mitochondrial localization [14]. Under these conditions, H₂O₂ also induces a massive mitochondrial division [14].

Mitochondria are major sources of ROS, and their replication and maintenance depend on the fission, fusion and segregation of pre-existing organelles. Mitochondria change their morphology throughout the cell cycle, and actively divide to allow proper segregation to daughter cells during mitosis [15]. Mitochondrial division, also a mechanism to segregate damaged parts for their posterior degradation by mitophagy [16], is coordinated by membrane-associated proteins, influenced by interactions with the actin cytoskeleton and other organelles [17] such as the endoplasmic reticulum (ER), and executed by dynamin-related proteins (Drp1 in humans and other animals; DnmA in *A. nidulans*). These GTPases, which are highly conserved in all eukaryotes, oligomerize in ring-like structures around the mitochondrial tubules, where GTP hydrolysis induces a conformational change that allows mitochondrial division [18–20]. Mutations in Drp1 and DnmA cause embryonic lethality in mice [21] and drastic defects in growth and development in *A. nidulans* [22], respectively. Moreover, defects in mitochondrial division are associated to different human pathologies [23]. In *Saccharomyces cerevisiae* and other fungi, Dnm1 is recruited to mitochondria by the adaptor protein Fis1 (FisA in *A. nidulans*) together with adaptors Mdv1 and Caf4 [24–26]. In *A. nidulans*, H₂O₂-induced mitochondrial division is totally dependent on DnmA and its receptor FisA [22].

A. nidulans is an excellent model to study cell biology processes during growth and cell differentiation, as it undergoes both asexual and sexual development. Vegetative hyphae are highly polarized cells that undergo branching and grow at the tips. Asexual development (conidiation) involves the formation of complex conidiophore structures. During this process, conidiophore stalk cells grow for a fixed length towards the air interface and then develop a multinucleated vesicle, from which uninucleate cells called metulae emerge. Metulae differentiate into conidiogenic cells called phialides, which produce long chains of uninucleate spores (conidia) by a series of mitotic divisions [27]. Actively growing hyphae from mutants lacking DnmA or FisA produce very long, tubular mitochondria, which fail to undergo division. Nevertheless, at the vesicle stage, mitochondria form highly convoluted structures that branch through developing metulae and phialides in a process that results in the partitioning of a single mitochondrion to every developed conidia [22].

Here, we show that even in the absence of DnmA or FisA, H₂O₂ induces major changes in mitochondrial morphology, characterized by an extensive production of mitochondrial constrictions that are preceded by mitochondrial depolarization. We show that calcium and ERMES complex subunit MdmB are required for mitochondrial constriction and division but not for depolarization or H₂O₂-induced changes in the mitochondrial outer membrane. In addition, H₂O₂ elicited changes in the endoplasmic reticulum (ER) and nuclear morphology that were similar to those observed during conidiophore development.

2. Materials and Methods

2.1. Strains, Media, and Growth Conditions

The *Aspergillus nidulans* strains used in this work are listed in Table S1. All of the strains were grown at 37 °C in 1% glucose–nitrate solid minimal medium [28], plus supplements.

2.2. Gene Deletion and Organelle Labelling

In order to delete the *mdmB* gene (AN6901), a construction was made using double-joint PCR [29], different combinations of primers (Table S2), and genomic DNA as a template. Two PCR fragments were generated using primers 5'ForMdmB/5'RevMdmB and 3'ForMdmB/3'RevMdmB. The *Aspergillus fumigatus pyrG* gene, used as selective marker, was amplified from plasmid PFNO3 [30] with primers PyrGForward and PyrGReverse. These three fragments were purified, mixed and used in a fusion PCR with primers

5'NestMdmB and 3'NestMdmB. The final 3856 bp *mdmB*–*AfpyrG*–*mdmB* cassette was purified and used to transform *A. nidulans* strains CDV02 and CVG29 by electroporation [31,32]. Several heterokaryons were obtained in three different transformations, three of which were analyzed by PCR and maintained on selective medium.

In order to label the endoplasmic reticulum, the wild-type strain (CLK43) was transformed with plasmid pAM01 [33], which contains ER-signal and ER-retention sequences from *Podospira anserina* BiP chaperone protein fused to GFP, expressed from *A. nidulans* *gpdA* promoter. The presence of labelled ER was confirmed by epifluorescence microscopy in strain TVG6. Strains TVG6 and CVG8 (with labelled mitochondria) were crossed to obtain strain CVG34, containing ER labelled with GFP and mitochondria labelled with mCherry. Strains CVG34 and TVG1($\Delta dnmA$) were crossed to obtain CVG32 ($\Delta dnmA$ with labelled ER and mitochondria). Strains CVG32 and CVG27 were crossed to obtain strains CVG46 (WT) and CVG47 ($\Delta dnmA$) with labelled ER, mitochondria and nuclei. In order to obtain strains with labelled mitochondrial outer membranes, strain CDV1, which expresses Tom20 [34] homolog AN0559 fused to GFP, from the *A. nidulans* *gpdA* promoter [35], was crossed with strain CVG1. From this cross, strains CVG45 ($\Delta dnmA$ with matrix and outer-membrane labelled mitochondria) and CVG48 ($\Delta dnmA$ with labelled mitochondrial outer membrane) were obtained. In all cases, the *dnmA* deletion for was confirmed by PCR.

2.3. Confocal and Airyscan Microscopy

The images were captured using a Zeiss LSM800 inverted laser scanning confocal microscope (Carl Zeiss, Jena, Germany) using a Plan Apochromat 63 \times /1.4 oil immersion objective and 405, 488 and 561 laser lines, according to the fluorescent tag. The Airyscan images were obtained with a LSM800 microscope and a Plan-Apochromat 63 \times /1.4 oil DIC M27 objective, using the Airyscan detectors (Carl Zeiss, Jena, Germany), with a 32-channel array of GaAsP detectors configured at 1.25 airy units per channel. Airyscan microscopy uses a confocal detection system that more efficiently collects light, increasing the signal-to-noise ratio and image speed acquisition, which results in higher resolution imaging than conventional confocal microscopy. All of the observations were conducted at 35 °C. The images were processed using software Zen 2012 (Carl Zeiss, Jena, Germany) and ImageJ 2 (v2.030/1.53f, K. W. Elicerei, Madison, USA). For fixed images, the samples were incubated with 300 μ L of a 1:100 dilution of stock fixing solution (2.46 M paraformaldehyde, 0.44 M EGTA, 0.5 M MgCl₂, 100 mM PIPES pH 6.9) for 3 min, rinsed three times with water, and observed using epifluorescence or confocal microscopy. TMRM (tetramethylrhodamine, methyl ester) was used to detect mitochondrial membrane potential [36]. A 10 mM stock solution prepared in DMSO was maintained frozen. Then, 100 μ M working solutions were prepared with water and used to cover sections of solid medium containing growing mycelia, for 20 min at 37 °C. The TMRM solution was removed and mycelia was treated or not with 5 mM H₂O₂, and observed using confocal microscopy. A 1 mM CCCP (Carbonyl cyanide *m*-chlorophenyl hydrazone, Sigma Aldrich, St. Louis, USA) stock solution was prepared in ethanol and maintained frozen. A 10 μ M working solution was prepared with water and used to cover sections of solid medium containing growing mycelia for 20 min. After this, the samples were rinsed three times with water and observed using confocal microscopy. Permeant calcium chelator BAPTA-AM (Invitrogen, Waltham, MA, USA) was prepared in DMSO as a 15 mM stock solution, and was maintained frozen. Then, 200 μ M working solutions prepared with water were used to cover mycelial samples for 2 h at 37 °C. After this, BAPTA-AM was removed, and the samples were rinsed with water and treated or not with 5 mM H₂O₂ for 20 min. Then, the samples were fixed or observed using confocal microscopy. All of the hyphal observations were restricted to growing tips, in order to avoid changes in mitochondrial morphology due to senescence or starvation. For the conidiophore imaging, the growing edge of a colony grown for 3 days at 37 °C was sectioned, a drop of water was added, and the section was carefully covered with a coverslip. Fields with early development conidiophores and a well-preserved structure were chosen for observation using confocal microscopy.

3. Results

3.1. H_2O_2 and CCCP Induce Mitochondrial Constriction and Membrane Depolarization

We have shown that non-lethal concentrations of H_2O_2 induce widespread mitochondrial division in *A. nidulans* wild-type strains, and that proteins DnmA and FisA are necessary for this process [22]. The results in Figure S1 confirm that H_2O_2 induces the production of individual round mitochondria, which do not recover the filamentous form within the experimental time frame or even longer incubation times. We detected that in the absence of DnmA or FisA, H_2O_2 was still able to induce changes in mitochondrial morphology. In order to study these changes, we initially used 18-h grown mycelia from $\Delta dnmA$ and $\Delta fisA$ mutants with mCherry matrix labelled mitochondria. These mutants were treated or not with 5 mM H_2O_2 for 20 min. Then, H_2O_2 was removed and the mycelia were incubated for another 10 min. After this, the mycelia were immediately fixed and multiple hyphal tips were observed using confocal microscopy. In the absence of H_2O_2 , the mitochondria from both $\Delta dnmA$ and $\Delta fisA$ mutants maintained a regular, filamentous form in 84–86% of the hyphal tips observed. However, a few isolated constriction-like structures were observed in 14–16% of the hyphal tips. In sharp contrast, in H_2O_2 -treated samples, 81 and 79% of the hyphal tips from $\Delta dnmA$ and $\Delta fisA$ mutants contained mitochondria with multiple constriction-like structures, respectively (Figure S2). These results suggested that without H_2O_2 , the mitochondria suffered some spontaneous and transient constrictions, and that the frequency of these constrictions was drastically increased by H_2O_2 . In order to test this, we followed this process in vivo using the same experimental conditions. Indeed, without H_2O_2 , most $\Delta dnmA$ mitochondria maintained a filamentous form during the observation period (0–300 s). In contrast, H_2O_2 induced the formation of round structures and mitochondrial constriction-like structures between 0 and 180 s, which became less defined between 240 and 300 s when the filamentous form started to recover (Figure 1, top panels). Similar phenomena were observed in the $\Delta fisA$ mutant, although mitochondrial constriction-like structures were more evident between 120 and 240 s, and the filamentous morphology started to recover around 300 s (Figure 1, bottom panels).

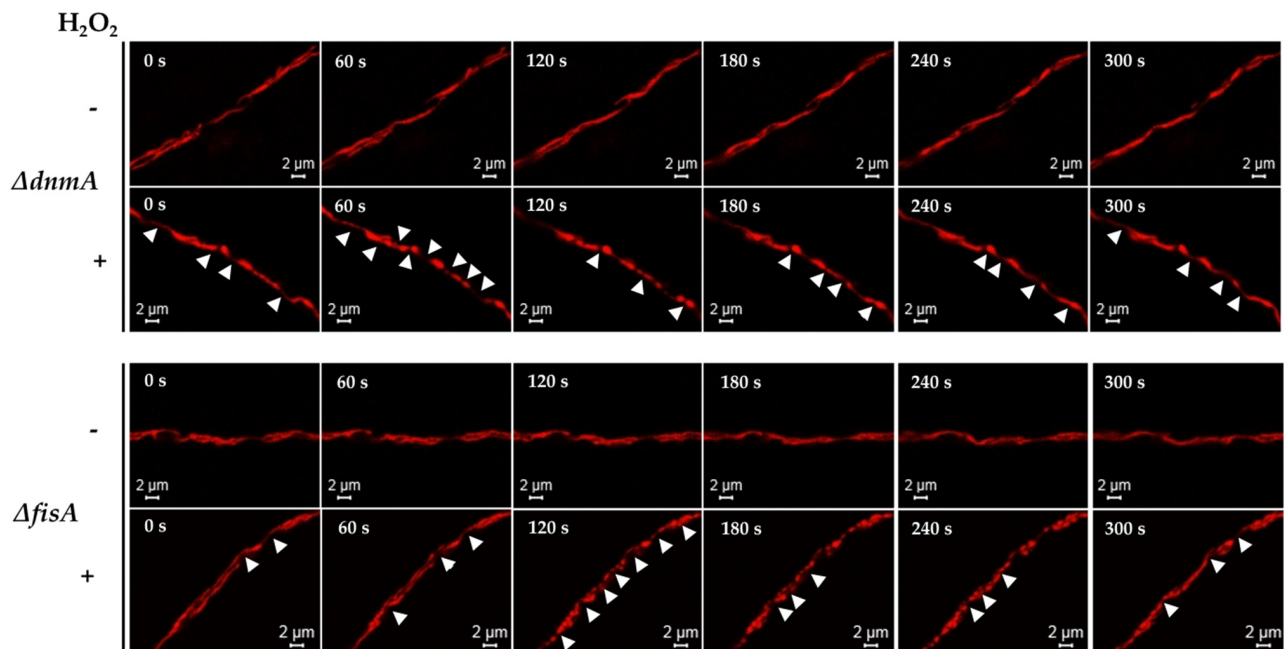


Figure 1. H_2O_2 induces transient mitochondrial constrictions in the absence of the mitochondrial fission machinery. Mycelia from $\Delta dnmA$ (CVG1) and $\Delta fisA$ (CVG2) mutant strains grown for 18 h were treated or not with 5 mM H_2O_2 for 20 min. After this, H_2O_2 was removed; after another 10-min incubation, hyphae were observed at the indicated times using confocal microscopy. The mitochondrial matrix is labelled with mts::mCherry. The arrowheads point to some of the constriction events.

In order to explore whether the H₂O₂-induced constriction-like structures were related to mitochondrial membrane depolarization, we first exposed a wild-type strain to carbonyl cyanide *m*-chlorophenylhydrazone (CCCP), a well-known oxidative phosphorylation uncoupler [37]. Like H₂O₂, CCCP was able to induce a massive mitochondrial division in a wild-type background, and the mitochondria did not recover their filamentous form after prolonged incubation times (Figure S1). When $\Delta dnmA$ and $\Delta fisA$ mutants were treated with CCCP, it induced mitochondrial constriction-like structures in 87 and 89% of the hyphal tips observed in both $\Delta dnmA$ and $\Delta fisA$ mutants, respectively (Figure S2). Observations in vivo showed that CCCP induced constriction-like structures much faster than H₂O₂, and that the changes in mitochondrial morphology were more dramatic in the $\Delta fisA$ mutant (Figure 2). Notably, these CCCP-induced changes were not reversible, and the round structures remained up to 400 s and beyond. Because H₂O₂ induces similar responses in $\Delta dnmA$ and $\Delta fisA$ mutants, we decided to focus our analysis using only $\Delta dnmA$ mutants. In order to follow mitochondrial depolarization more directly, we incubated $\Delta dnmA$ mutant cells—in which the outer mitochondrial membrane was labelled with GFP—in the presence of the voltage sensor tetramethylrhodamine methyl-ester (TMRM), which is rapidly sequestered by the negatively charged mitochondrial membrane potential. The results in Figures 3 and S3 show that after this incubation, about 95% of the hyphae contained TMRM-stained mitochondria. Under these conditions, H₂O₂ induced a gradual loss of mitochondrial membrane potential. After 5, 8, 15 and 20 min in H₂O₂, the number of hyphae stained with TMRM decreased to 87, 76, 20 and 6%, respectively. In contrast, in the presence of CCCP, mitochondrial membrane potential was lost after only 5 min of incubation (Figure 3). The use of strains with GFP-labelled outer mitochondrial membrane (Figure 3, Figure 4, Figure S4 and Figure S5) allowed us to confirm that the mitochondrial constriction-like structures observed in Figures 1 and 2 correspond to actual constrictions present in non-dividing mitochondria; they will be named as such. Notably, H₂O₂-induced mitochondrial constrictions were evident at around 15 min, while with CCCP they were already present after 5 min (Figure 3).

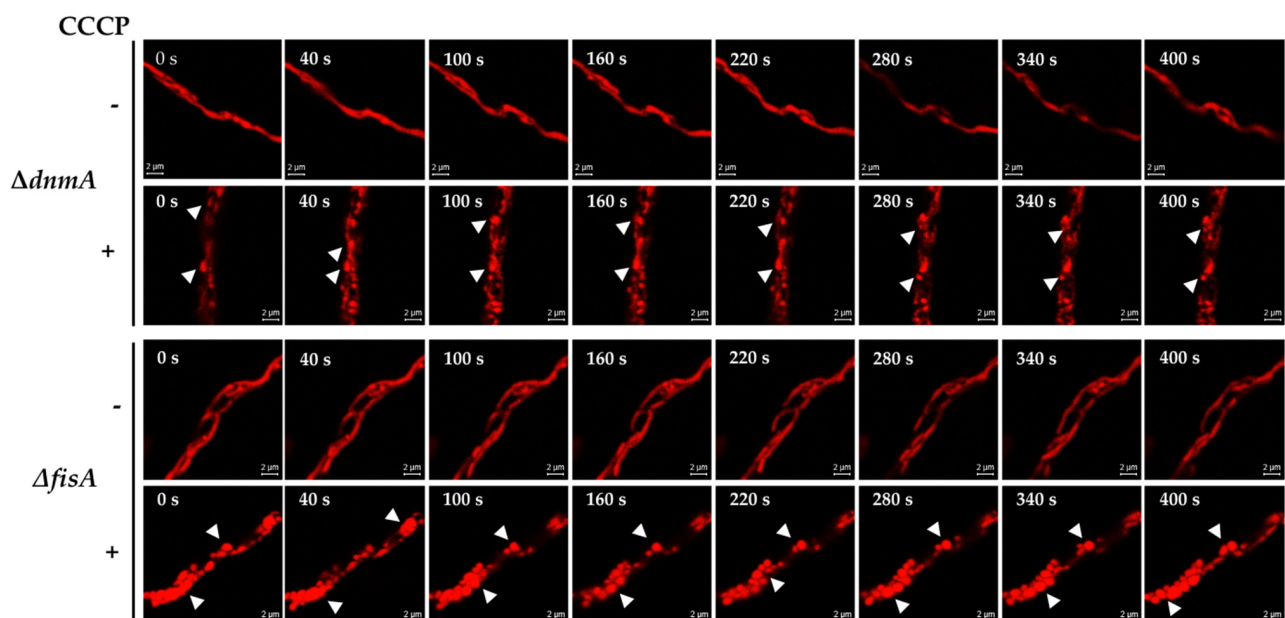


Figure 2. Uncoupler CCCP induces irreversible mitochondrial constrictions in the absence of the mitochondrial fission machinery. Mycelia from $\Delta dnmA$ (CVG1) and $\Delta fisA$ (CVG2) mutant strains grown for 18 h were treated or not with 10 μ M CCCP for 20 min. After this, CCCP was removed, and the hyphae were incubated for another 10 min and observed at the indicated times using confocal microscopy. The mitochondrial matrix is labelled with mts::mCherry. The arrowheads point to some of the round structures produced by mitochondrial constrictions.

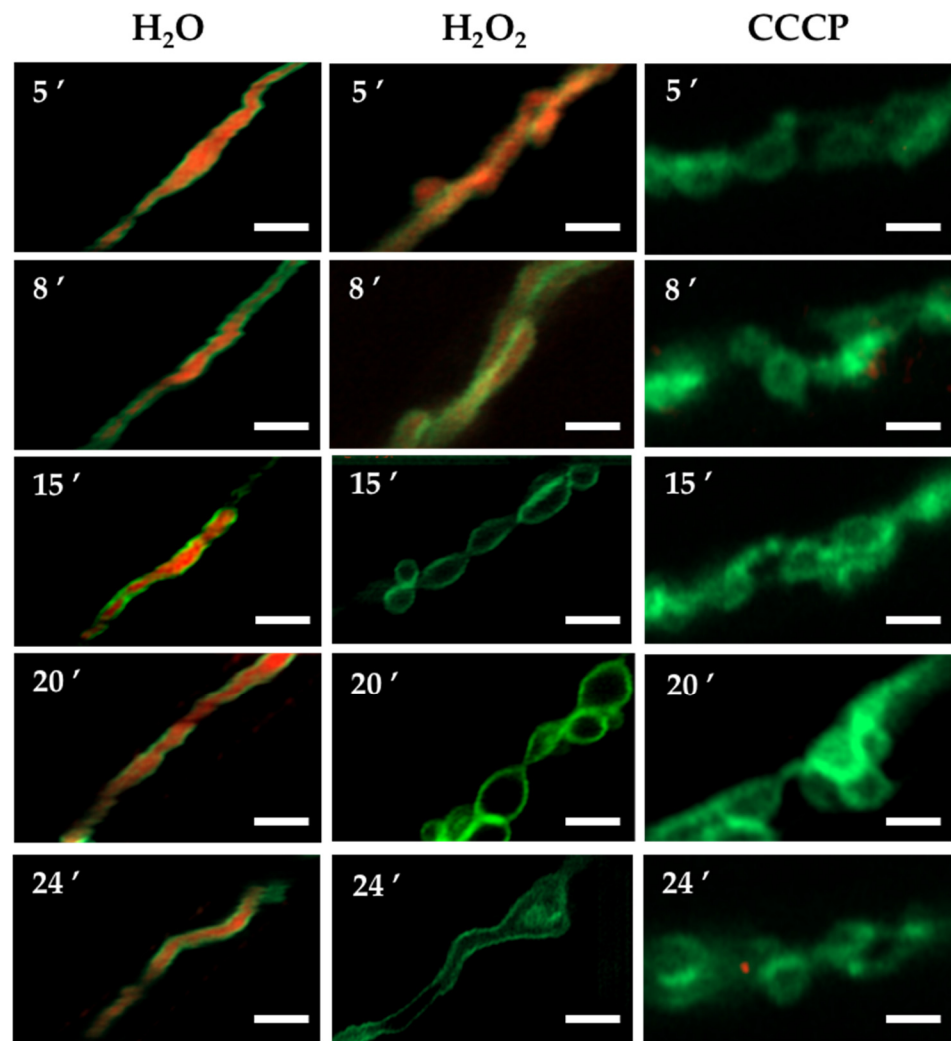


Figure 3. H_2O_2 induces a gradual depolarization of the mitochondria before extensive mitochondrial constrictions are observed. Mycelia from $\Delta dnmA$ *tom20::gfp* strain CVG48 were grown for 18 h at 37°C and stained with $100\ \mu\text{M}$ TMRM for 20 min. After this, samples were rinsed three times with distilled water and then treated or not with $5\ \text{mM}$ H_2O_2 or $10\ \mu\text{M}$ CCCP for another 20 min, rinsed, and immediately observed using Airyscan microscopy. The red fluorescence signal corresponds to TMRM-stained mitochondria, and the green signal corresponds to GFP-labelled mitochondrial outer membrane. Scale bar = $2\ \mu\text{m}$.

We used the $\Delta dnmA$ strain with labelled matrix and outer mitochondrial membrane to follow the changes in both compartments induced by H_2O_2 . The results in Figure 4 show that H_2O_2 induced both transient and more permanent changes in mitochondrial morphology within a short time frame. Indeed, the filamentous mitochondria went from a series of globular structures connected by thin filaments of external membrane, back to a filamentous form. In contrast, after most of the constrictions disappeared, the mitochondrial outer membrane presented major rearrangements, including the formation of mitochondrial branching points and septum-like structures (Figures 4 and S4), as well as donut-like structures (Figure S4). Figure 4 also shows that although most constrictions produce globular shapes of similar size, some smaller round shapes were also produced. CCCP, in addition to irreversible mitochondrial constrictions, also induced the major reshaping of the mitochondrial outer membrane (Figure S5).

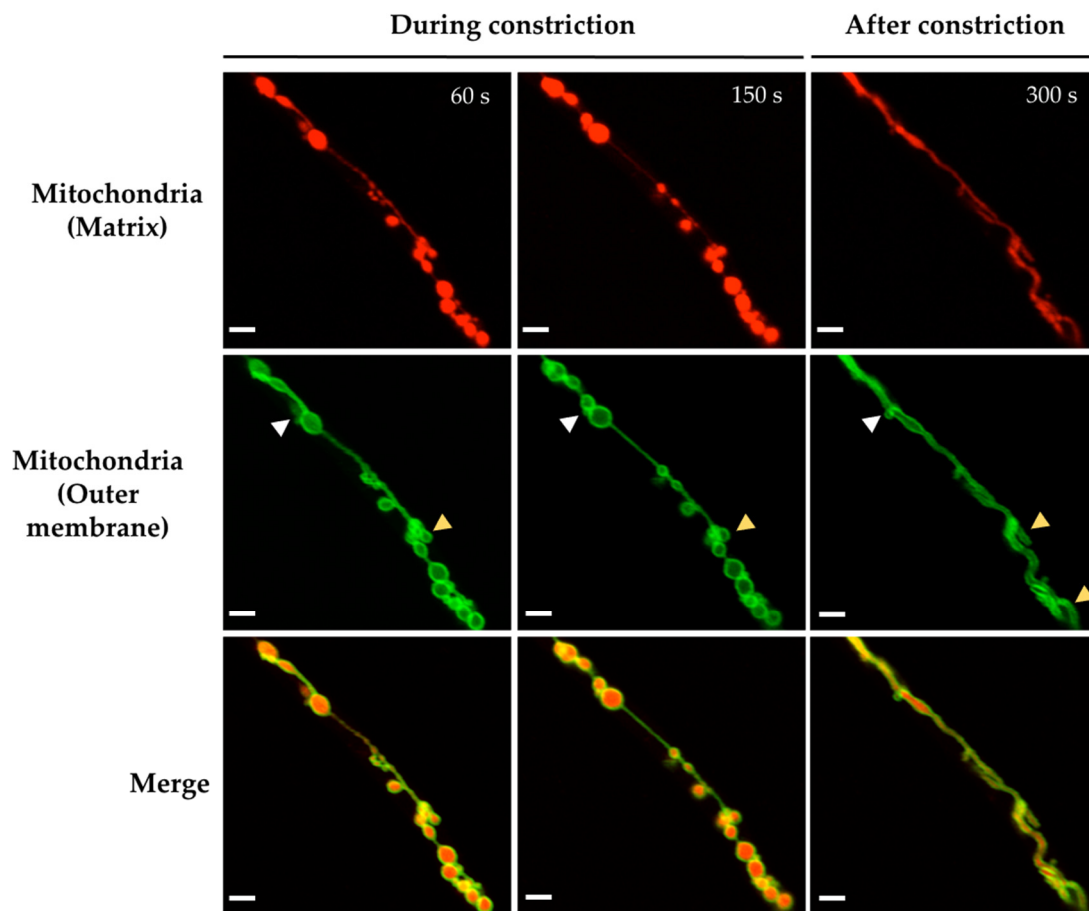


Figure 4. H_2O_2 induces mitochondrial branching and the major reshaping of the outer mitochondrial membrane. Mycelia from $\Delta dnmA$ (CVG45) mutant strain were grown for 18 h and then treated with 5 mM H_2O_2 for 20 min. H_2O_2 was removed, and after another 10 min of incubation, hyphae were observed at the indicated times using Airyscan microscopy. The white and yellow arrowheads point to septum-like and branching structures, respectively. Scale bar = 2 μm .

Our results indicate that H_2O_2 induces a generalized and transient mitochondrial constriction response prior to actual division, which involves gradual membrane depolarization, as well as major rearrangements of the outer mitochondrial membrane, some of which appear to be related to mitochondrial branching.

3.2. H_2O_2 -Induced Mitochondrial Constriction Sites Are in Contact with the Endoplasmic Reticulum

Previous studies have established that close contact between mitochondria and the endoplasmic reticulum (ER) is important for mitochondrial division [17,38,39]. In order to examine mitochondria–ER interactions during H_2O_2 -induced mitochondrial constrictions, we generated $\Delta dnmA$ strain CVG32, in which the mitochondria and ER were labelled with mCherry and GFP, respectively. The *in vivo* H_2O_2 experiments in Figure 5A show that before the constrictions were evident (0 s), the ER appeared as a filamentous network around the mitochondrial filament, with some ER regions adjacent to or in contact with the mitochondrial filament. Between 60 and 120 s, mitochondrial constrictions became evident, and the ER appeared surrounding some of these constrictions and in closer contact with mitochondria. Between 300 and 360 s, the mitochondria’s filamentous shape started to recover, and mitochondria–ER interactions became less evident. In order to better appreciate these interactions in the absence of organelle movement, we decided to make observations in mycelia fixed immediately after the H_2O_2 treatment. The results in Figure 5B show several instances in which the ER was clearly surrounding or interacting

with mitochondrial constrictions. Under these conditions, at least two different types of mitochondria–ER interactions could be identified: 1, cases in which the ER was encompassing a mitochondrial constriction and 2, cases in which the ER clearly co-localized with the globular structures produced by the constriction of mitochondria. In addition to these changes, we appreciated that the structure of the ER was modified by the H₂O₂ treatment. As seen in Figure 5A, the ER network developed dotted structures between 60 and 360 s, which were more evident around putative round nuclear structures. In order to confirm this, we repeated the experiment using a strain in which the nuclei were labelled with BFP. The results in Figure 6A show that in the wild-type strain, H₂O₂ induced the formation of a few ER-dotted structures. However, these were not increased around nuclei. In contrast, and as observed before in the $\Delta dnmA$ mutant (Figure 5A), H₂O₂ led to an increased ER signal around nuclei and the production of ER-dotted structures, which were more evident in the nuclear boundary. Additionally, in both strains, H₂O₂ induced clear changes in nuclear morphology, from an elongated to a rounded shape. When the fluorescence signal intensity was used to calculate the total ER and nuclear area, the ER area was lower in the $\Delta dnmA$ mutant compared to the WT strain, suggesting that the lack of DnmA and the resulting tubular mitochondrial morphology seem to affect the shape and extension of the ER network. The presence of H₂O₂ further decreased the ER area in the $\Delta dnmA$ mutant, while H₂O₂ induced a reduction in the nuclear area in both the WT and $\Delta dnmA$ strains (Figure 6B).

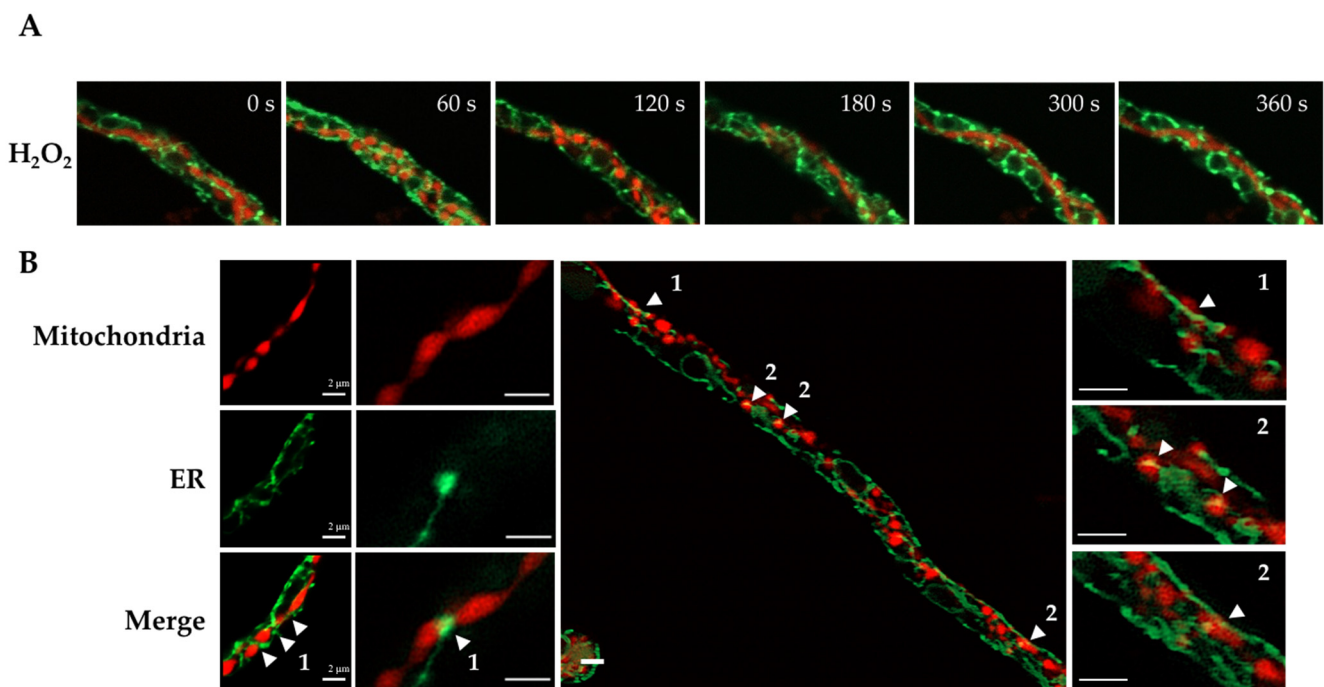


Figure 5. H₂O₂-induced mitochondrial constriction sites are in close contact with the endoplasmic reticulum. Mycelia from $\Delta dnmA$ (CVG32) mutant strain was grown for 18 h and treated with 5 mM H₂O₂ for 20 min. H₂O₂ was removed, and after a 10-min additional incubation, hyphae were observed at the indicated times using confocal microscopy. (A) Changes in the mitochondria–ER morphology after H₂O₂ treatment. (B) Magnification of the mitochondria–ER contacts during H₂O₂-induced mitochondrial constrictions. The samples were treated as in (A), fixed, and observed using Airyscan microscopy. Labels 1 and 2 point to examples of different types of mitochondria–ER interactions. The red and green signals correspond to mitochondria labelled with mCherry and ER labelled with GFP, respectively. The arrowheads point to mitochondria–ER contacts. Scale bar = 2 μ m.

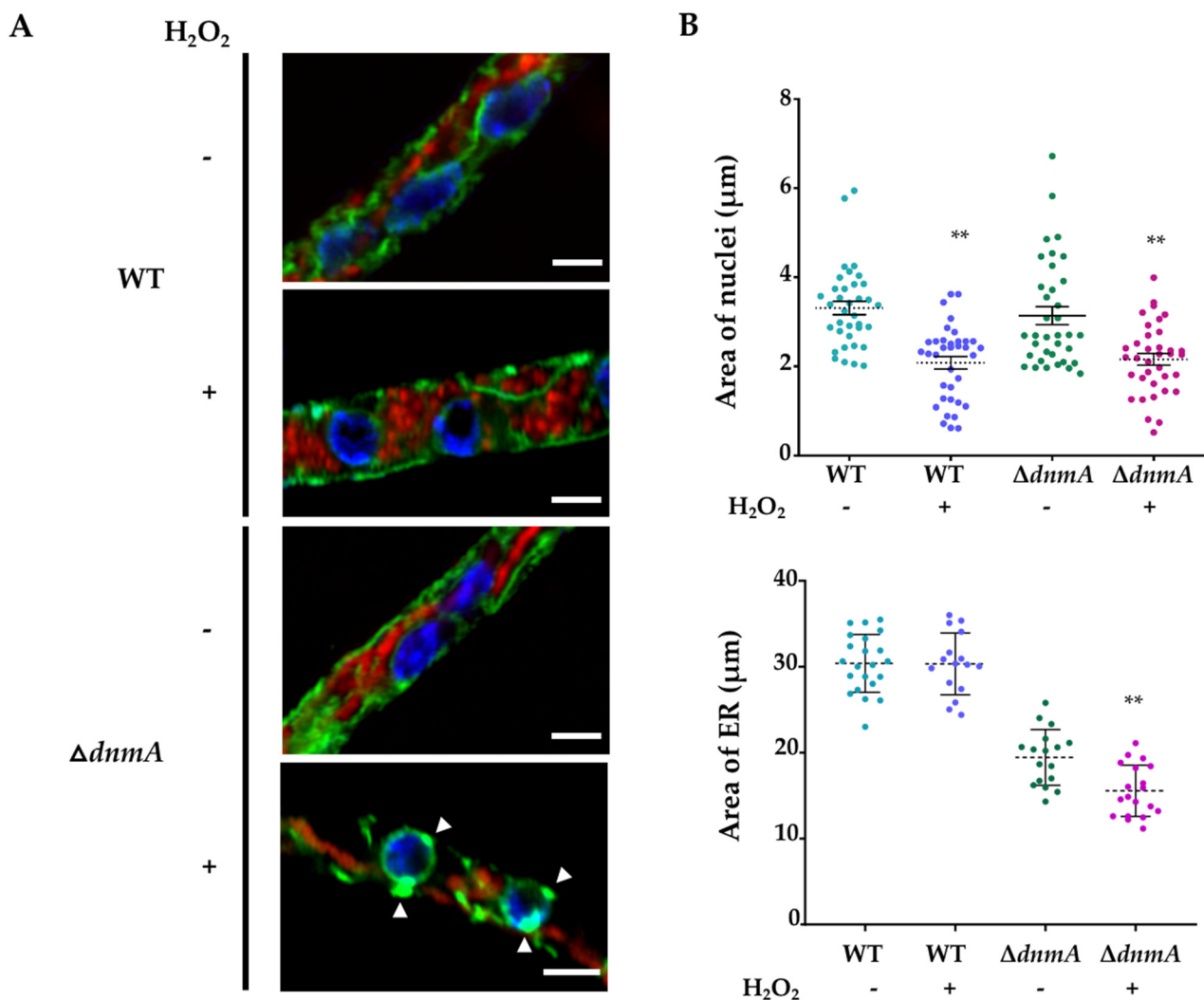


Figure 6. H₂O₂ induces morphological changes in mitochondria, ER and nuclei. (A) Mycelia from WT (CVG46) and $\Delta dnmA$ (CVG47) strains grown for 18 h were treated or not with 5 mM H₂O₂ for 20 min. H₂O₂ was removed, and after a 10 min of additional incubation, hyphae were observed using Airyscan microscopy. (B) The area of 35 nuclei from WT and $\Delta dnmA$ strains treated or not with H₂O₂ was determined. Under the same conditions, the total ER area from 35 hyphal tips was determined (** $p < 0.001$ by t -test). The red, green and blue signals correspond to mitochondria labelled with mCherry, ER labelled with GFP, and nuclei labelled with BFP, respectively. The white arrowheads point to ER-dotted structures around nuclei. Scale bar = 2 μ m.

In summary, our results show that the ER maintains close contacts with mitochondria even in the absence of division, and that in multiple cases the ER is localized around the mitochondrial constrictions induced by H₂O₂, suggesting that mitochondria–ER contacts are necessary in order to produce this H₂O₂-induced response. Moreover, we show that H₂O₂ induces drastic changes in nuclear structure and, in the absence of mitochondrial division, it induces the formation of ER dot-like structures, particularly around the nuclei.

3.3. Mitochondrial Constrictions and ER-Dotted Structures Are Formed during Asexual Development

We have proposed that cell differentiation is a response to increased cellular ROS levels [1,2]. Consistent with this idea, we observed that an extensive mitochondrial division is produced not only in response to external H₂O₂, but also during conidiophore development. Moreover, in the absence of mitochondrial division, an extensive branching of mitochondria is produced during this differentiation process, allowing the inheritance of

a single mitochondrion to the asexual spores [22]. In order to determine whether mitochondrial and ER morphological changes similar to those induced by H_2O_2 were detected under physiological conditions, we analyzed the morphology of these organelles at early stages of conidiophore development. The results in Figure 7 show the presence of mitochondrial constrictions at the conidiophore stalk and vesicle developmental stages. Under these conditions, the ER formed an intricate network, parts of which surrounded the nuclei or were found interacting with mitochondria at both the filaments and constriction points. ER dot-like structures were also observed in some cases around the nuclei, which in general presented rounded, rather than elongated, shapes.

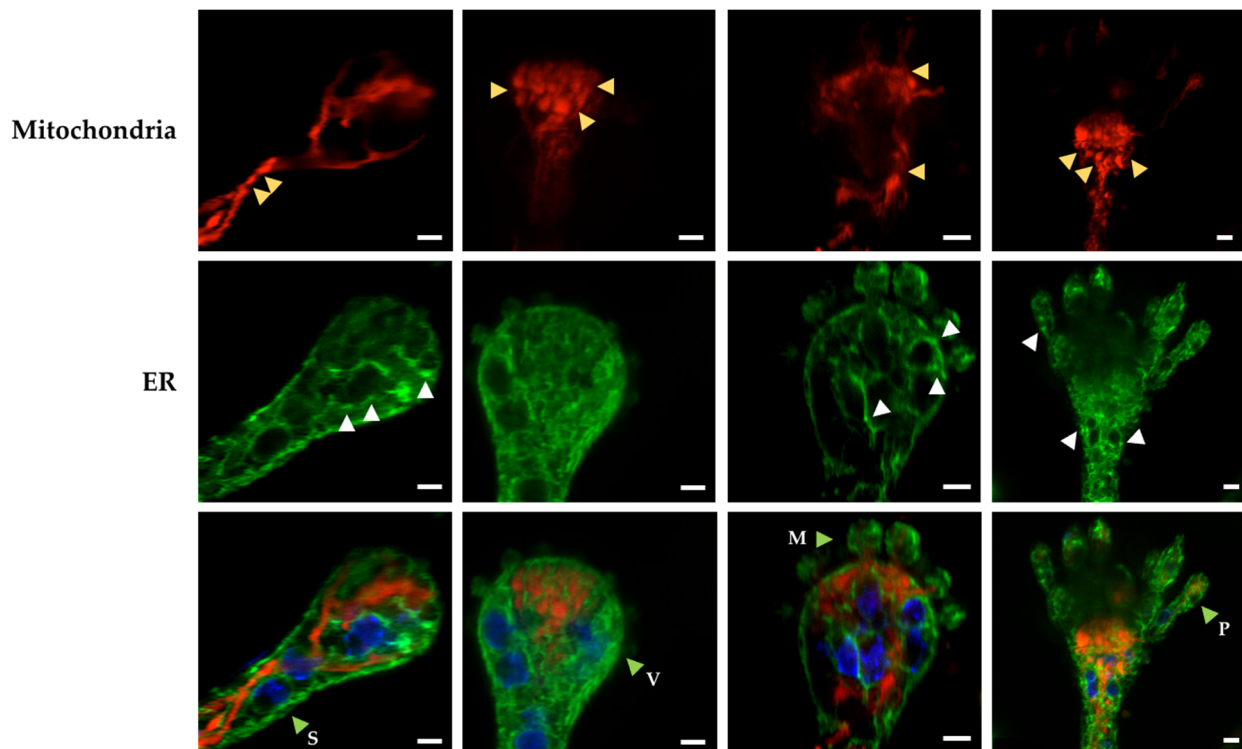


Figure 7. Mitochondrial constrictions and ER-dotted structures are produced during normal conidiophore development. The growing edge of an $\Delta dnmA$ (CVG47) colony grown for 3 days was sectioned, and its conidiophores were observed using Airyscan microscopy. The red, green and blue signals correspond to mitochondria labelled with mCherry, ER labelled with GFP, and nuclei labelled with BFP, respectively. The yellow arrowheads point to constricted mitochondria; white arrowheads indicate ER-dotted structures. The green arrowheads point to conidiophore stalks (S), vesicles (V), metulae (M) and phialides (P). Scale Bar = 2 μ m.

These results show that mitochondria, ER and nuclei undergo morphological changes during asexual development that are similar to those induced by H_2O_2 during hyphal growth. This suggests that H_2O_2 produced under physiological conditions during normal growth and conidiophore development might impact organelle function—including the regulation of mitochondrial constriction and division—at mitochondria–ER interaction points.

3.4. Calcium Is Required for Mitochondrial Constrictions Induced by H_2O_2 or CCCP but Not for the Remodeling of the Mitochondrial Outer Membrane

Mitochondria and the ER make intimate contacts that are necessary for mitochondrial dynamics and in order to exchange calcium (Ca^{2+}) and lipids [40]. In order to explore whether Ca^{2+} was necessary for H_2O_2 -induced mitochondrial constriction, we used BAPTA-AM, a cell-permeant, highly specific Ca^{2+} chelator. $\Delta dnmA$ mutant cells were incubated with BAPTA-AM for 2 h and then treated or not with H_2O_2 or CCCP for 20 min, and were observed using confocal microscopy. The incubation with BAPTA-AM alone did not

notably affect the tubular morphology of the mitochondria (Figure S6A). Remarkably, the preincubation with BAPTA-AM prevented the formation of mitochondrial constrictions in response to both H_2O_2 and CCCP (Figures S6B and S7). Because H_2O_2 also induced major rearrangements of the mitochondrial external membrane (Figures 4 and S4), we asked whether BAPTA-AM was also able to prevent these changes. The results in Figure 8 show that $\Delta dnmA$ tubular mitochondria usually contain a few regions where the mitochondrial outer membrane looks condensed, and the number of these regions was barely affected by the presence of BAPTA-AM. Like before, H_2O_2 did not induce mitochondrial constrictions in hyphae pretreated with BAPTA-AM. However, H_2O_2 was still able to induce major remodeling of the mitochondrial outer membrane, which was apparent in the formation of circular structures (Figure 8, lower panels). These results indicate that H_2O_2 induces mitochondrial constriction and outer membrane rearrangement by two different pathways.

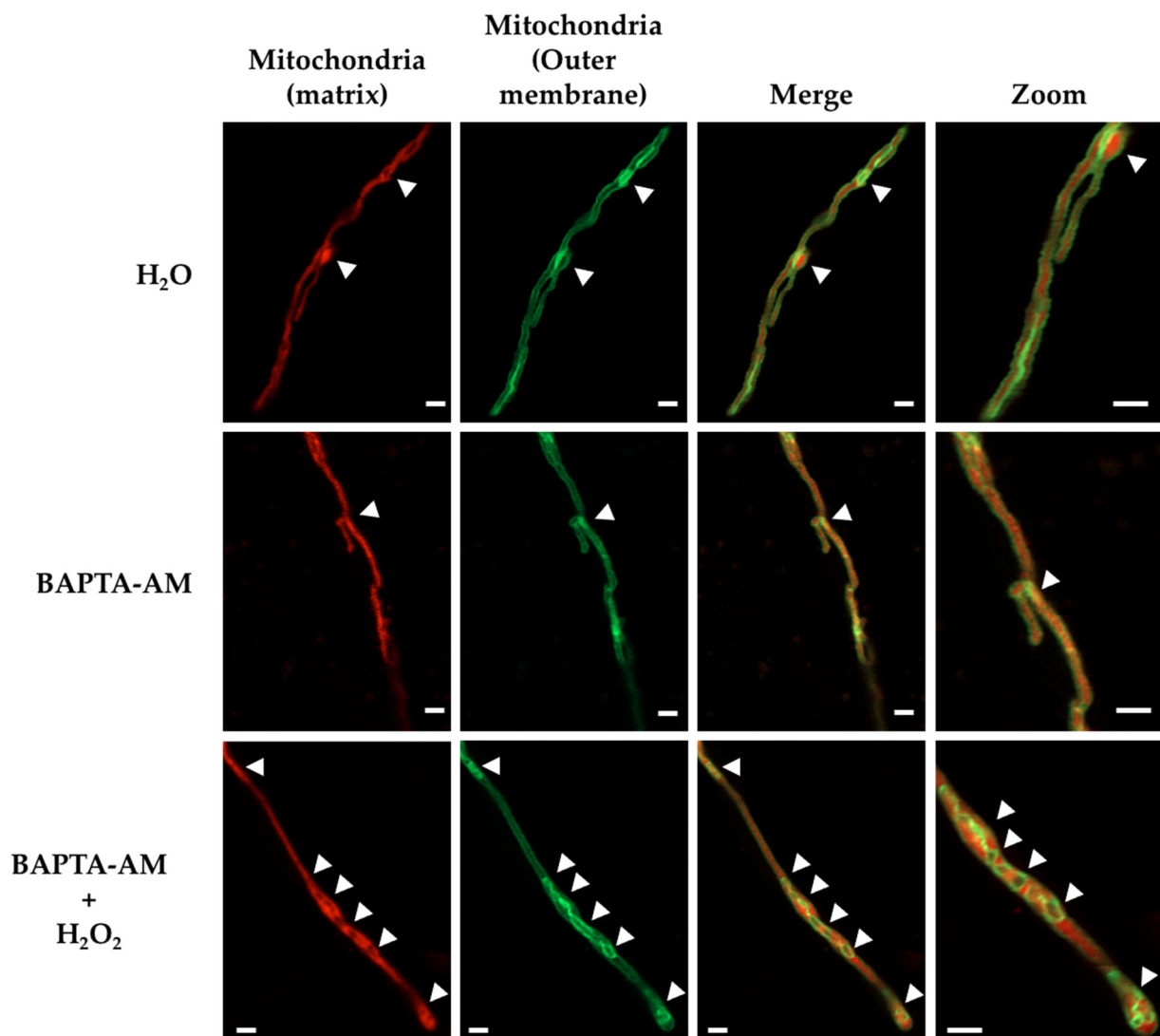


Figure 8. BAPTA-AM prevents mitochondrial constriction induced by H_2O_2 but not the remodeling of the mitochondrial outer membrane. Mycelia from the $\Delta dnmA$ (CVG45) strain were grown for 18 h, incubated with 200 μM BAPTA-AM for 2 h, rinsed with sterile water, treated or not with 5 mM H_2O_2 for 20 min, and then observed using Airyscan microscopy. The arrowheads indicate regions where the mitochondrial outer membrane is condensed or forms circular structures. Scale bar = 5 μm .

3.5. *MdmB*, a Subunit of the ERMES Complex, Is Required for Mitochondrial Constriction and Division

The *S. cerevisiae* ER–mitochondria encounter structure (ERMES) is a tethering complex composed by proteins Mdm10, Mmm1, Mdm43 and Mdm12; it is critical for ER–mitochondrial interactions [41]. In *A. nidulans*, the protein MdmB (AN6901) corresponds to *S. cerevisiae* Mdm10 [42]. In order to analyze the importance of the ERMES complex and ER–mitochondria interactions in H₂O₂-induced mitochondrial constriction and division, we decided to generate $\Delta mdmB$ mutants using the *Afp_{pyrG}* gene as selective marker (Figure S8A). However, after multiple attempts, we were only able to obtain transformants with heterokaryotic morphology (i.e., colonies with irregular growth sectors and heterogeneous conidiation), suggesting that *mdmB* was an essential gene in *A. nidulans* (Figure S8B). Indeed, this was confirmed by using PCR to corroborate the heterokaryotic nature of three independent transformants. When conidia from these heterokaryons were plated on selective media, lacking uridine/uracil, the WT conidia failed to germinate, while the $\Delta mdmB$ conidia were able to germinate and form a short germ tube that failed to grow any further (Figure S8C). This allowed us to determine the terminal phenotype of $\Delta mdmB$ mutants with respect to mitochondria and ER morphologies. As shown in Figure 9A, $\Delta mdmB$ mutant germlings contain a few globular mitochondria, instead of the more filamentous mitochondria normally seen in WT strains under these conditions. Notably, these globular mitochondria did not show clear contacts with the ER.

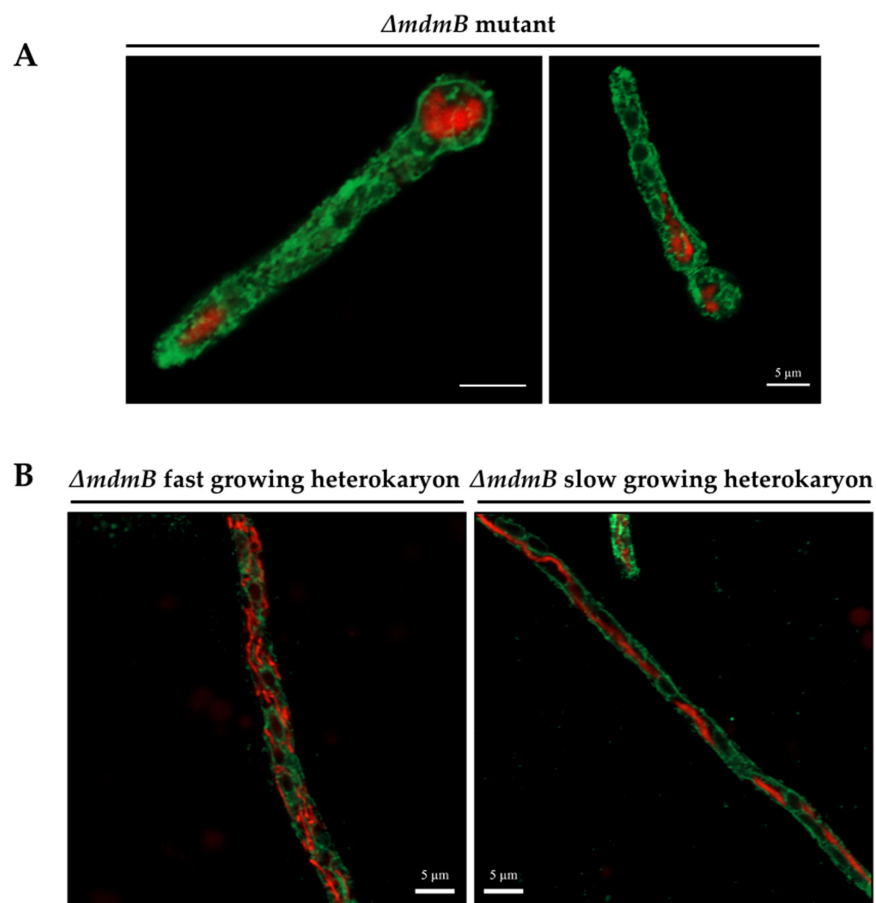


Figure 9. MdmB is required for mitochondrial division. (A) Spores from $\Delta mdmB$ heterokaryon HVG2 were plated on selective media at 37 °C by 21 h. Then, the conidia were fixed and observed using Airyscan microscopy. (B) Fast-growing and slow-growing mycelial sectors, obtained from a $\Delta mdmB$ HVG2 heterokaryotic colony grown on selective media for 5 days, were fixed and observed using confocal microscopy. The red and green signals correspond to mitochondria labelled with mCherry and ER labelled with GFP, respectively. Scale bar = 5 μ m.

In order to determine the effects of different MdmB dosages on mitochondrial morphology, we compared fast-growing and slow-growing mycelial sectors obtained from $\Delta mdmB$ heterokaryotic colonies grown on selective media. The results in Figure 9B (left panel) show that the fast-growing sectors contained mitochondria with a wild-type morphology composed of a filamentous and branched network and some smaller individual mitochondria. The ER was observed as a complex network intertwined with the mitochondrial network. In contrast, slow-growing sectors contained some hyphae in which a single mitochondrial filament was observed, similar to those observed in $\Delta dnmA$ and $\Delta fisA$ mutants, while the ER formed a simpler and mainly cortical linear network, where mitochondria–ER contacts were not as evident.

Using the same approach, we asked whether MdmB was necessary to induce the mitochondrial constrictions elicited by H_2O_2 . In vivo experiments using hyphae from $\Delta mdmB$ slow-growing heterokaryotic sectors with tubular mitochondria (Figure 10A) showed that the mitochondria and the ER filamentous form remained virtually unchanged for the observation period (0–324 s). When these sectors were exposed to H_2O_2 , the mitochondria preserved most of their filamentous form, and only two incipient constrictions were observed between 202 and 243 s at putative mitochondria–ER contact points (Figure 10B). Similarly, CCCP was also largely ineffective to induce mitochondrial constrictions in tubular mitochondria from $\Delta mdmB$ slow-growing heterokaryotic sectors (Figure S9). These results reveal that MdmB is necessary for the development of mitochondrial constrictions induced by either H_2O_2 or CCCP.

All of the long mitochondrial filaments observed in $\Delta mdmB$ hyphae from slow growing heterokaryotic sectors were found to accumulate ROS when stained with the superoxide reporter MitoSox Red (Figure 11A), which is consistent with our previous results showing that the lack of mitochondrial division results in an increased production of mitochondrial ROS [22]. As shown in Figure 11B, $\Delta mdmB$ heterokaryon tubular mitochondria were stained with TMRM and depolarized by the addition of H_2O_2 , indicating that mitochondria–ER contacts mediated by the ERMES complex are needed for H_2O_2 -induced mitochondrial constriction but not for initial H_2O_2 -induced mitochondrial membrane depolarization. Notably, although mitochondrial constrictions were not observed under these conditions, H_2O_2 was still able to induce the major reshaping of the outer mitochondrial membrane.

In summary, our results indicate that *A. nidulans* ERMES complex component MdmB is an essential protein that mediates contacts between mitochondria and the ER, and that these contacts are necessary for H_2O_2 -induced mitochondrial early constriction and later division but not for the rearrangement of the outer mitochondrial membrane. The fact that Ca^{2+} is necessary for H_2O_2 -induced mitochondrial constriction but not for the remodeling of the outer mitochondrial membrane (Figure 8) supports a model in which H_2O_2 regulates the transport of Ca^{2+} between the ER and the mitochondria to regulate mitochondrial constriction and division.

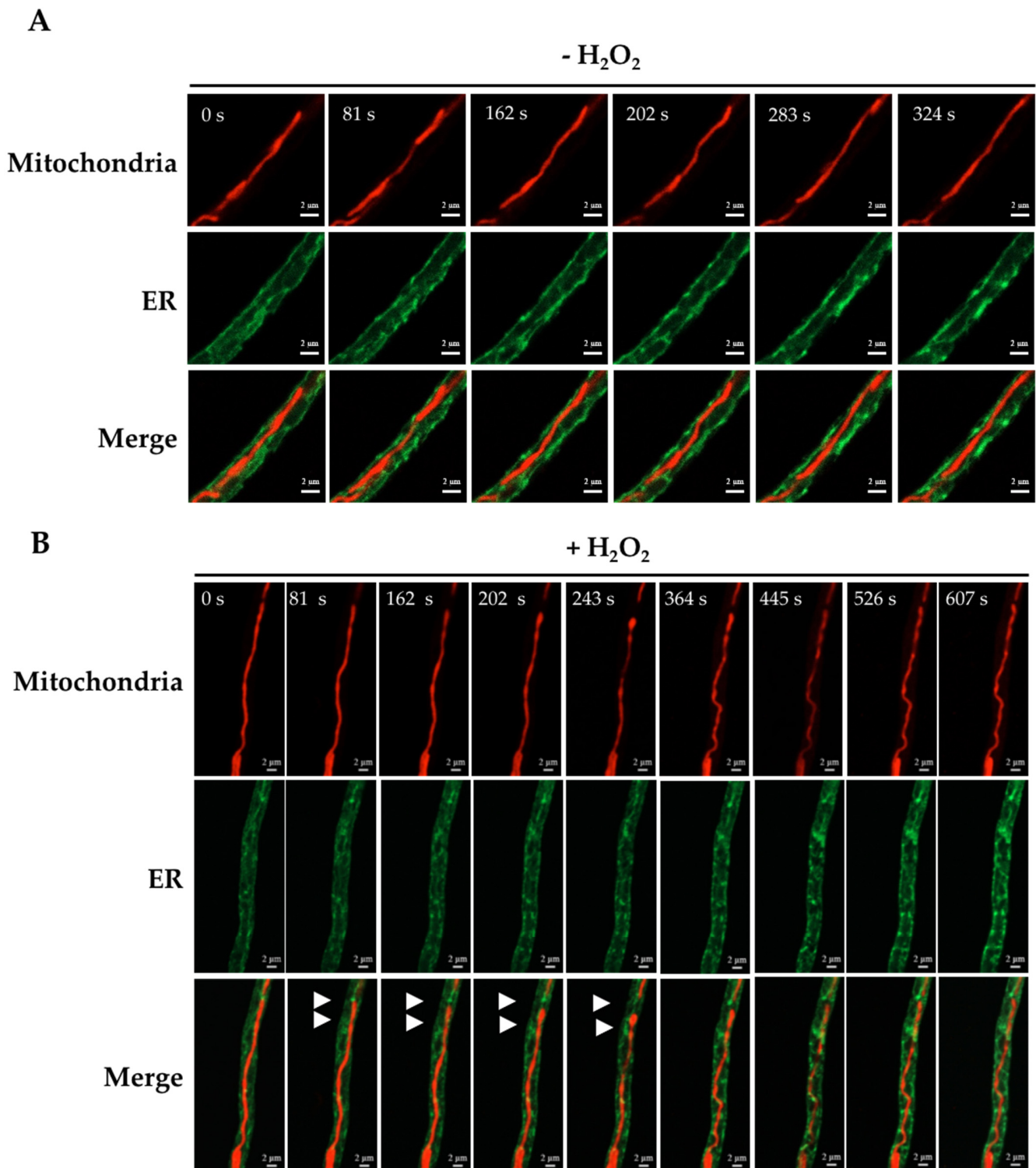


Figure 10. Mitochondria–ER contacts are essential in order to produce mitochondrial constrictions in response to H₂O₂. Mycelia from a slow-growing section from $\Delta m d m B$ heterokaryon HGV2, grown on selective media for 5 days, was treated (B) or not (A) with 5 mM H₂O₂ for 30 min, and was then observed for the indicated times using confocal microscopy. The white arrowheads in (B) point to a ER–mitochondria contact point where an incipient mitochondrial constriction is observed.

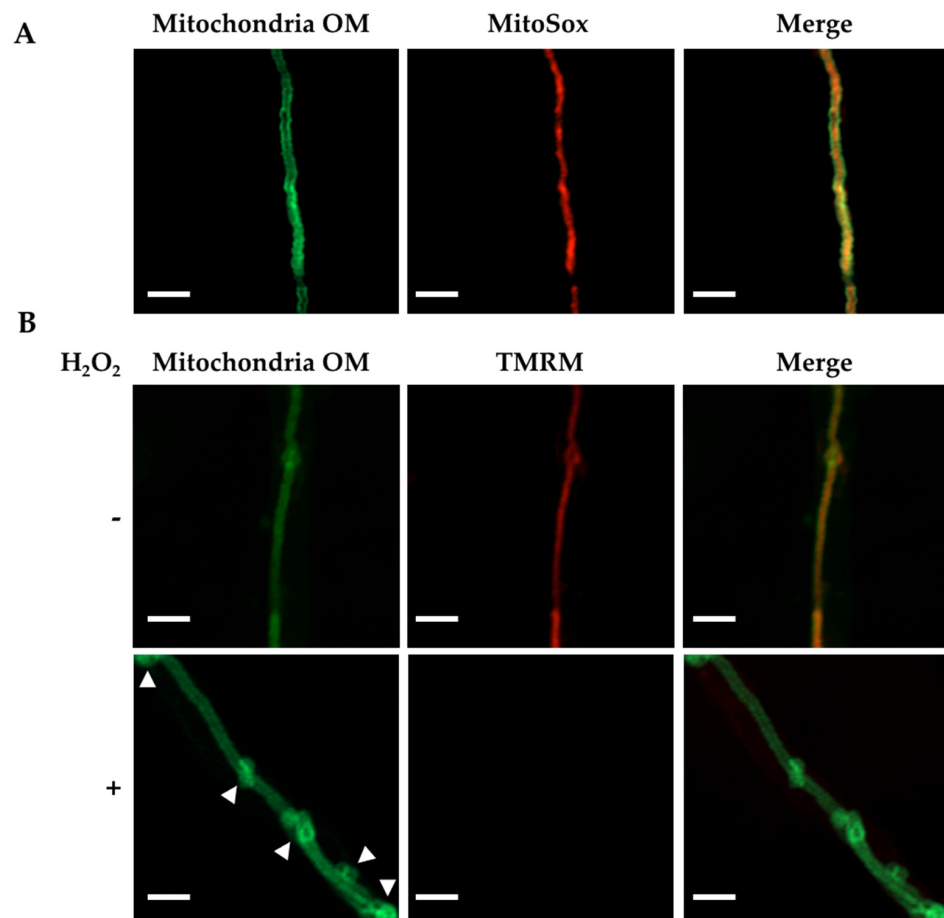


Figure 11. Tubular mitochondria from $\Delta m d m B$ heterokaryons show ROS accumulation, and in response to H_2O_2 lose membrane potential and undergo the major reshaping of the outer mitochondrial membrane. (A) Mycelia from a slow-growing sector from a $\Delta m d m B$ heterokaryon HVG3 colony grown on selective media for 5 days were stained with MitoSox for 10 min, rinsed with sterile water, and observed using Airyscan microscopy. (B) Mycelia obtained as in (A) were stained with TMRM for 20 min, rinsed with water, and treated or not with 5 mM H_2O_2 for 30 min. The samples were observed using Airyscan microscopy. The white arrowheads indicate rearrangements of the mitochondrial outer membrane (OM). Scale bar = 5 μ m.

4. Discussion

4.1. H_2O_2 Induces Mitochondrial Depolarization, Constriction and Rearrangements of the Outer Mitochondrial Membrane

H_2O_2 and CCCP induce extensive mitochondrial division in *A. nidulans* and other eukaryotes. However, earlier events occurring before actual mitochondrial division are difficult to appreciate in a wild-type background. Using mutants impaired in mitochondrial division, we found that these two compounds induce a profuse production of mitochondrial constrictions as well as the reshaping of the outer mitochondrial membrane. CCCP induced rapid depolarization and a generalized formation of mitochondrial constrictions in a process that was irreversible. H_2O_2 induced gradual depolarization followed by widespread formation of mitochondrial constrictions in a process that was reversible within a few minutes. In addition, the formation of isolated, spontaneous and reversible constrictions was observed in the course of normal growth. These results suggest that the mitochondrial constrictions which are normally present during regular growth result from local depolarization events, the frequency of which is markedly increased by H_2O_2 . In any case, the dramatic changes in mitochondrial morphology induced by external H_2O_2 involve the presence of H_2O_2 perception mechanisms that should also function under normal conditions.

Lee and Yoon reported the occurrence of transient contractions of the mitochondrial matrix that were notably increased by a lack of mitochondrial division. However, these authors proposed that contractions led to a reversible loss of inner membrane potential [43]. We did not observe that the lack of mitochondrial division per se resulted in an extensive production of mitochondrial constrictions. Moreover, in the presence of both H₂O₂ and CCCP, the loss of inner membrane potential preceded the massive production of mitochondrial constrictions. Our results indicate that in the absence of H₂O₂, contractions are not generalized, despite the apparent continuity of the mitochondrial filaments present when DnmA, FisA or MdmB are absent. This might be related to the fact that individual cristae within the same mitochondrion have different membrane potentials and are functionally independent [44]. More recently, Cho et al. reported that the spontaneous and repetitive constriction of the mitochondrial inner compartment (CoMIC) was associated with a subsequent division in neurons, supporting the idea that CoMICs are priming events for efficient mitochondrial division. However, in their experiments, CoMICs were observed in the internal mitochondrial membrane independently of outer mitochondrial morphological changes [45]. We generally observed that H₂O₂-induced mitochondrial constrictions involved both internal and outer mitochondrial membranes. However, H₂O₂ induced additional changes in the outer mitochondrial membrane that remained after the mitochondrial tubular shape was restored, which resulted in the formation septum and donut-like structures, and in some cases led to mitochondrial branching.

In addition to its effects on mitochondrial morphology, H₂O₂ induced the formation of ER dot-like structures and the rounding of nuclei. Notably, similar changes were observed in conidiophore vesicles for asexual sporulation. In a wild-type background, mitochondria undergo extensive division at the vesicle stage [22]. In the absence of mitochondrial division, the observed extensive mitochondrial constrictions and branching are necessary to distribute mitochondria to the multiple metulae that differentiate from the vesicle, and from there to developing phialides and conidial cell types ([22] and this work). One possible interpretation is that H₂O₂ production increases during conidiophore development as a mechanism to regulate mitochondrial division and inheritance. Consistent with this is the fact that mutants lacking ROS-producing NADPH oxidase NoxA and its regulatory subunit NoxR are not only blocked in sexual development [6,46] but also show decreased asexual sporulation [46].

4.2. Intracellular Ca²⁺ and MdmB, a Subunit of the ERMES Complex, Are Required for H₂O₂-Induced Mitochondrial Constriction and Division

Our results show that mitochondrial depolarization by CCCP or H₂O₂ is not enough to induce mitochondrial constrictions, and that intracellular calcium is essential for this process. This is consistent with the fact that, in animal cells, CoMICs occurred at potential division sites contacting the ER, and the intra-mitochondrial influx of Ca²⁺ induced and potentiated CoMIC formation [45].

Indeed, we observed that the ER is in close contact with mitochondria even in the absence of division, and that in many cases the ER is localized around the mitochondrial constrictions induced by H₂O₂. Moreover, we showed that MdmB, an ortholog of *S. cerevisiae* ERMES complex subunit Mdm10, is involved in maintaining contact between the ER and mitochondria, and is critical for H₂O₂-induced mitochondrial constriction and division. The elimination of components of the ERMES complex has different consequences in different fungi, but generally mitochondrial morphology is affected. In *A. nidulans*, MdmB was found to be an essential protein. Previously, *A. nidulans* mutants with a partially deleted *mdmB* gene were reported as viable, although with reduced growth at 37 °C. However, at a low temperature these mutants contained both tubular and giant non-motile mitochondria [42], suggesting that these mutants expressed a MdmB polypeptide with partial function. The characterization of *A. fumigatus* conditional mutants in all four core ERMES components and *mdm10* and *mdm12* deletion mutants showed that each component was critical for growth, and that the downregulation of each component produced cells with

giant as well as very small mitochondria [47]. Similarly, in our experiments, the terminal phenotype of $\Delta mdmB$ mutants was characterized for the formation of ball-like bloated mitochondria. The downregulation of MdmB in slow-growing heterokaryons resulted in a novel phenotype characterized by a lack of mitochondrial division and the production of tubular mitochondria with increased ROS levels, exactly as occurs in non-dividing mitochondria from $\Delta dnmA$ and $\Delta fisA$ mutants. A defective mitochondrial division could explain the defects in mitochondrial inheritance observed in *S. cerevisiae mdm10* mutants [48].

4.3. H_2O_2 Differential Roles in Mitochondrial Dynamics

Our results show that H_2O_2 affects mitochondrial function in at least three different aspects. It induces gradual membrane depolarization, mitochondrial constriction and outer membrane remodeling. Although interrelated, these processes can be separated, as shown by the fact that Ca^{2+} and a close contact between mitochondria and ER are necessary for mitochondrial constriction but not for mitochondrial depolarization or the reshaping of the outer membrane. ROS have also been reported as affecting mitochondrial distribution and mobility, but these effects were independent of cytoplasmic Ca^{2+} or the mitochondrial membrane potential [49].

The relationship between mitochondrial membrane depolarization, ROS and Ca^{2+} is a complex subject [50,51]. For instance, CCCP-induced mitochondrial depolarization led to an increased oxidation of nuclear DNA in animal cells, suggesting an increased production of ROS under these conditions [51]. On the other hand, there is evidence indicating that transient depolarization can lead to the suppression of ROS production [52]. In addition, non-dividing mitochondria, either because they lack DnmA, FisA [22] or MdmB (this work), contain increased levels of superoxide and perhaps other ROS, which seem to show a heterogenous concentration within mitochondria.

Despite this, it is known that the low-conductance mitochondrial permeability transition pore regulates the flux of Ca^{2+} and ROS out of the mitochondrial matrix, whilst the accumulation of Ca^{2+} in the mitochondrial matrix induces the opening of a high-conductance mitochondrial permeability transition pore. While mitochondria experience brief depolarization events or flickerings that contribute to the generation of ROS, the opening of the high conductance permeability transition pore leads to complete and persistent mitochondrial depolarization and the redistribution of ions and solutes up to 1.5 kDa across the internal mitochondrial membrane, and a more generalized production of ROS [53]. Although not in connection to mitochondrial constriction and membrane remodeling, a recent publication relates mitochondrial depolarization, ROS and Ca^{2+} signaling between mitochondria and the ER. Boot et al. (2021) reported that transient depolarizations of individual mitochondria, initiated by openings of the permeability transition pore, generate oxidative bursts at the ER–mitochondrial interface. Such oxidative bursts constitute a mitochondria–ER signaling pathway by sensitizing ER redox-sensitive IP3R Ca^{2+} release channels. These authors also proposed that metabolic stress could amplify local ER–mitochondria proximity signals to larger regions of the cell [54].

According to this, our results are consistent with a model in which H_2O_2 would increase the frequency of flickering, leading to a gradual mitochondrial depolarization and an increased efflux of endogenous ROS. ROS produced by mitochondrial flickering would sensitize ER redox-sensitive Ca^{2+} release channels, inducing mitochondrial Ca^{2+} loading by the ER, eventually leading to the induction of high-conductance mitochondrial permeability transition in a reversible way, such that the mitochondrial constrictions are reversible. These initial events would be necessary but not sufficient to induce extensive mitochondrial constriction. This interplay between ROS and ER-derived Ca^{2+} can regulate mitochondrial constrictions by affecting actin polymerization. In animal cells, mitochondrial depolarization induces a rapid actin assembly around mitochondria by two parallel pathways, one of them involving cytoplasmic Ca^{2+} , PKCB, Rac, WRC and the Arp2/3 complex, which affects mitochondrial morphology by inhibiting mitochondrial circularization and the processing

of OPA1 [55]. A similar mechanism, initiated by H₂O₂, could result in the mitochondrial constrictions that we observe in *A. nidulans*.

We also found that H₂O₂ regulates mitochondrial outer membrane remodeling by a mechanism that is independent of Ca²⁺ and mitochondrial–ER contacts. It is likely that such membrane reshaping results from the mitochondrial membrane fusion events that normally precede mitochondrial division [56]. It is known that different types of stress activate mitochondrial fusion in animal cells in a process regulated by mitofusins Mfn1 and Mfn2, located in the mitochondrial outer membrane, and by Opa1, located in the inner mitochondrial membrane. Notably, oxidized glutathione disulfide promotes the assembly of higher-order Mfn complexes, mediated by reversible disulfide bonds [57,58]. However, Fzo1 proteins, the functional equivalents of animal Mfn in fungi, lack the two conserved cysteines that are essential for Mfn-redox regulation, which led to the suggestion that stress-induced mitochondrial fusion is a specific adaptation to multicellular life [57]. However, our results suggest that alternative mechanisms for a redox regulation of mitochondrial outer membrane fusion are present in fungi. Therefore, although the necessity of mitochondrial constriction for proper Drp1/DnmA oligomerization around mitochondria and their subsequent division seems conserved in fungi and animals, the mechanisms triggering and accomplishing mitochondrial constriction might be different. Here, it is interesting to note that similarly to bacterial division, and in contrast to animal cells, mitochondrial constriction in the red algae *Cyanidioschyzon merolae* is mediated by the protein FtsZ [19,59]. In any case, our results indicate that H₂O₂ is a critical signal that regulates mitochondrial dynamics by regulating mitochondrial membrane depolarization, constriction, and outer membrane remodeling.

Supplementary Materials: The following supporting information can be downloaded at: <https://www.mdpi.com/article/10.3390/jof8080829/s1>. Table S1: *Aspergillus nidulans* strains used in this work; Table S2: Primers used in this work; Figure S1: H₂O₂ and CCCP induce mitochondrial division in *A. nidulans*; Figure S2: Number of hyphae containing filamentous or constricted mitochondria in $\Delta dnmA$ and $\Delta fisA$ mutants; Figure S3: Number of hyphae showing TMRM-stained mitochondria in $\Delta dnmA$ mutants treated with H₂O₂; Figure S4: H₂O₂ induces transient mitochondrial constrictions and the irreversible reshaping of the mitochondrial outer membrane, including the formation of donut-like and septum-like structures; Figure S5: CCCP induces irreversible mitochondrial constrictions and the major reshaping of mitochondrial outer membrane; Figure S6: BAPTA-AM does not affect the mitochondrial filamentous form but prevents mitochondrial constriction induced by H₂O₂ or CCCP; Figure S7: BAPTA-AM prevents mitochondrial constriction induced by H₂O₂ or CCCP; Figure S8: PCR confirmation of $\Delta mdmB$ heterokaryons and the terminal phenotype of $\Delta mdmB$ mutants; Figure S9: Filamentous mitochondria from $\Delta mdmB$ heterokaryons do not form constrictions in the presence of CCCP.

Author Contributions: Conceptualization, investigation, formal analysis, writing—original draft preparation, V.G.-B.; conceptualization, supervision, formal analysis, writing—original draft preparation, project administration, funding acquisition, J.A. All authors have read and agreed to the published version of the manuscript.

Funding: This research was funded by CONACYT grant CONACYT-DFG 277869, and UNAM grants PAPIIT-UNAM IN215622 and IV200519.

Institutional Review Board Statement: Not applicable.

Informed Consent Statement: Not applicable.

Data Availability Statement: Not applicable.

Acknowledgments: We are grateful to Biologist Olivia Sánchez (IFC-UNAM) and Abraham Rosas for technical assistance. We thank Daniela Campiño for strain CDV1, and Arturo Hernández (IFC-UNAM) and Arturo Jiménez (IQ-UNAM) for the generous donation of BAPTA-AM and TMRM, respectively. We also acknowledge support and technical help from Imagenology, Molecular Biology and Computer IFC-UNAM facilities.

Conflicts of Interest: The authors declare no conflict of interest.

References

1. Aguirre, J.; Rios-Momberg, M.; Hewitt, D.; Hansberg, W. Reactive oxygen species and development in microbial eukaryotes. *Trends Microbiol.* **2005**, *13*, 111–118. [[CrossRef](#)] [[PubMed](#)]
2. Hansberg, W.; Aguirre, J. Hyperoxidant states cause microbial cell differentiation by cell isolation from dioxygen. *J. Theor. Biol.* **1990**, *142*, 201–221. [[CrossRef](#)]
3. Cano-Dominguez, N.; Alvarez-Delfin, K.; Hansberg, W.; Aguirre, J. NADPH oxidases NOX-1 and NOX-2 require the regulatory subunit NOR-1 to control cell differentiation and growth in *Neurospora crassa*. *Eukaryot. Cell* **2008**, *7*, 1352–1361. [[CrossRef](#)]
4. Cano-Dominguez, N.; Bowman, B.; Peraza-Reyes, L.; Aguirre, J. *Neurospora crassa* NADPH Oxidase NOX-1 Is Localized in the Vacuolar System and the Plasma Membrane. *Front. Microbiol.* **2019**, *10*, 1825. [[CrossRef](#)] [[PubMed](#)]
5. Dirschnabel, D.E.; Nowrousian, M.; Cano-Dominguez, N.; Aguirre, J.; Teichert, I.; Kuck, U. New Insights Into the Roles of NADPH Oxidases in Sexual Development and Ascospore Germination in *Sordaria macrospora*. *Genetics* **2014**, *196*, 729–744. [[CrossRef](#)] [[PubMed](#)]
6. Lara-Ortiz, T.; Riveros-Rosas, H.; Aguirre, J. Reactive oxygen species generated by microbial NADPH oxidase NoxA regulate sexual development in *Aspergillus nidulans*. *Mol. Microbiol.* **2003**, *50*, 1241–1255. [[CrossRef](#)]
7. Malagnac, F.; Lalucque, H.; Lepere, G.; Silar, P. Two NADPH oxidase isoforms are required for sexual reproduction and ascospore germination in the filamentous fungus *Podospora anserina*. *Fungal Genet. Biol.* **2004**, *41*, 982–997. [[CrossRef](#)]
8. Kawasaki, L.; Sanchez, O.; Shiozaki, K.; Aguirre, J. SakA MAP kinase is involved in stress signal transduction, sexual development and spore viability in *Aspergillus nidulans*. *Mol. Microbiol.* **2002**, *45*, 1153–1163. [[CrossRef](#)]
9. Mendoza-Martínez, A.E.; Cano-Dominguez, N.; Aguirre, J. Yap1 homologs mediate more than the redox regulation of the antioxidant response in filamentous fungi. *Fungal Biol.* **2019**, *24*, 253–262. [[CrossRef](#)]
10. Rhee, S.G. Redox signaling: Hydrogen peroxide as intracellular messenger. *Exp. Mol. Med.* **1999**, *31*, 53–59. [[CrossRef](#)]
11. Garrido-Bazan, V.; Jaimes-Arroyo, R.; Sanchez, O.; Lara-Rojas, F.; Aguirre, J. SakA and MpkC Stress MAPKs Show Opposite and Common Functions During Stress Responses and Development in *Aspergillus nidulans*. *Front. Microbiol.* **2018**, *9*, 2581. [[CrossRef](#)] [[PubMed](#)]
12. Lara-Rojas, F.; Sanchez, O.; Kawasaki, L.; Aguirre, J. *Aspergillus nidulans* transcription factor AtfA interacts with the MAPK SakA to regulate general stress responses, development and spore functions. *Mol. Microbiol.* **2011**, *80*, 436–454. [[CrossRef](#)] [[PubMed](#)]
13. Carrasco-Navarro, U.; Aguirre, J. H₂O₂ Induces Major Phosphorylation Changes in Critical Regulators of Signal Transduction, Gene Expression, Metabolism and Developmental Networks in *Aspergillus nidulans*. *J. Fungi* **2021**, *7*, 624. [[CrossRef](#)] [[PubMed](#)]
14. Jaimes-Arroyo, R.; Lara-Rojas, F.; Bayram, O.; Valerius, O.; Braus, G.H.; Aguirre, J. The SrkA Kinase Is Part of the SakA Mitogen-Activated Protein Kinase Interactome and Regulates Stress Responses and Development in *Aspergillus nidulans*. *Eukaryot Cell* **2015**, *14*, 495–510. [[CrossRef](#)] [[PubMed](#)]
15. Salazar-Roa, M.; Malumbres, M. Fueling the Cell Division Cycle. *Trends Cell Biol.* **2017**, *27*, 69–81. [[CrossRef](#)] [[PubMed](#)]
16. Kleele, T.; Rey, T.; Winter, J.; Zaganelli, S.; Mahecic, D.; Perreten Lambert, H.; Ruberto, F.P.; Nemir, M.; Wai, T.; Pedrazzini, T.; et al. Distinct fission signatures predict mitochondrial degradation or biogenesis. *Nature* **2021**, *593*, 435–439. [[CrossRef](#)]
17. Friedman, J.R.; Lackner, L.L.; West, M.; DiBenedetto, J.R.; Nunnari, J.; Voeltz, G.K. ER tubules mark sites of mitochondrial division. *Science* **2011**, *334*, 358–362. [[CrossRef](#)]
18. Bleazard, W.; McCaffery, J.M.; King, E.J.; Bale, S.; Mozdy, A.; Tieu, Q.; Nunnari, J.; Shaw, J.M. The dynamin-related GTPase Dnm1 regulates mitochondrial fission in yeast. *Nat. Cell Biol.* **1999**, *1*, 298–304. [[CrossRef](#)] [[PubMed](#)]
19. Kraus, F.; Roy, K.; Pucadyil, T.J.; Ryan, M.T. Function and regulation of the divisome for mitochondrial fission. *Nature* **2021**, *590*, 57–66. [[CrossRef](#)]
20. Tabara, L.C.; Morris, J.L.; Prudent, J. The Complex Dance of Organelles during Mitochondrial Division. *Trends Cell Biol.* **2021**, *31*, 241–253. [[CrossRef](#)]
21. Wakabayashi, J.; Zhang, Z.Y.; Wakabayashi, N.; Tamura, Y.; Fukaya, M.; Kensler, T.W.; Iijima, M.; Sesaki, H. The dynamin-related GTPase Drp1 is required for embryonic and brain development in mice. *J. Cell Biol.* **2009**, *186*, 805–816. [[CrossRef](#)]
22. Garrido-Bazan, V.; Pardo, J.P.; Aguirre, J. DnmA and FisA Mediate Mitochondria and Peroxisome Fission, and Regulate Mitochondrial Function, ROS Production and Development in *Aspergillus nidulans*. *Front. Microbiol.* **2020**, *11*, 837. [[CrossRef](#)] [[PubMed](#)]
23. Serasinghe, M.N.; Chipuk, J.E. Mitochondrial Fission in Human Diseases. *Handb. Exp. Pharmacol.* **2017**, *240*, 159–188. [[CrossRef](#)] [[PubMed](#)]
24. Griffin, E.E.; Graumann, J.; Chan, D.C. The WD40 protein Caf4p is a component of the mitochondrial fission machinery and recruits Dnm1p to mitochondria. *J. Cell Biol.* **2005**, *170*, 237–248. [[CrossRef](#)]
25. Tieu, Q.; Nunnari, J. Mdv1p is a WD repeat protein that interacts with the dynamin-related GTPase, Dnm1p, to trigger mitochondrial division. *J. Cell Biol.* **2000**, *151*, 353–365. [[CrossRef](#)] [[PubMed](#)]
26. Tieu, Q.; Okreglak, V.; Naylor, K.; Nunnari, J. The WD repeat protein, Mdv1p, functions as a molecular adaptor by interacting with Dnm1p and Fis1p during mitochondrial fission. *J. Cell Biol.* **2002**, *158*, 445–452. [[CrossRef](#)] [[PubMed](#)]
27. Timberlake, W.E.; Clutterbuck, A.J. Genetic regulation of conidiation. In *Aspergillus: 50 Years On*; Martinelli, S.D., Kinghorn, J.R., Eds.; Elsevier: Amsterdam, The Netherlands, 1994; Volume 29, pp. 283–427.
28. Hill, T.W.; Käfer, E. Improved protocols for *Aspergillus* minimal medium: Trace element and minimal medium stock solution. *Fungal Genet. Newsl.* **2001**, *48*, 20–21. [[CrossRef](#)]

29. Yu, J.H.; Hamari, Z.; Han, K.H.; Seo, J.A.; Reyes-Dominguez, Y.; Scazzocchio, C. Double-joint PCR: A PCR-based molecular tool for gene manipulations in filamentous fungi. *Fungal Genet. Biol.* **2004**, *41*, 973–981. [[CrossRef](#)] [[PubMed](#)]
30. Nayak, T.; Szewczyk, E.; Oakley, C.E.; Osmani, A.; Ukil, L.; Murray, S.L.; Hynes, M.J.; Osmani, S.A.; Oakley, B.R. A versatile and efficient gene-targeting system for *Aspergillus nidulans*. *Genetics* **2006**, *172*, 1557–1566. [[CrossRef](#)] [[PubMed](#)]
31. Sanchez, O.; Aguirre, J. Efficient transformation of *Aspergillus nidulans* by electroporation of germinated conidia. *Fungal Genet. Newsl.* **1996**, *43*, 48–51. [[CrossRef](#)]
32. Sanchez, O.; Navarro, R.E.; Aguirre, J. Increased transformation frequency and tagging of developmental genes in *Aspergillus nidulans* by restriction enzyme-mediated integration (REMI). *Mol. Gen. Genet.* **1998**, *258*, 89–94. [[CrossRef](#)]
33. Lopez-Fuentes, A.D.; Meizoso-Huesca, A.; Peraza-Reyes, L. An endoplasmic reticulum domain is associated with the polarized growing cells of *Podospira anserina* hyphae. *Fungal Genet. Biol.* **2020**, *137*, 103338. [[CrossRef](#)] [[PubMed](#)]
34. Pfanner, N.; Douglas, M.G.; Endo, T.; Hoogenraad, N.J.; Jensen, R.E.; Meijer, M.; Neupert, W.; Schatz, G.; Schmitz, U.K.; Shore, G.C. Uniform nomenclature for the protein transport machinery of the mitochondrial membranes. *Trends Biochem. Sci.* **1996**, *21*, 51–52. [[CrossRef](#)]
35. Campiño-Arias, D. La Proteína PxdA en el Transporte y la Función Peroxisomal Durante el Crecimiento y la Diferenciación Celular en el Hongo *Aspergillus nidulans*. Masters degree Thesis, Universidad Nacional Autónoma de México, México City, Mexico, 2022.
36. Hernandez-Juarez, C.; Flores-Cruz, R.; Jimenez-Sanchez, A. Fluorescent probe for early mitochondrial voltage dynamics. *Chem Commun.* **2021**, *57*, 5526–5529. [[CrossRef](#)] [[PubMed](#)]
37. Demine, S.; Renard, P.; Arnould, T. Mitochondrial Uncoupling: A Key Controller of Biological Processes in Physiology and Diseases. *Cells* **2019**, *8*, 795. [[CrossRef](#)] [[PubMed](#)]
38. Eisner, V.; Csordas, G.; Hajnoczky, G. Interactions between sarco-endoplasmic reticulum and mitochondria in cardiac and skeletal muscle—pivotal roles in Ca²⁺ and reactive oxygen species signaling. *J. Cell Sci.* **2013**, *126*, 2965–2978. [[CrossRef](#)]
39. Lang, A.B.; Peter, A.T.J.; Walter, P.; Kornmann, B. ER-mitochondrial junctions can be bypassed by dominant mutations in the endosomal protein Vps13. *J. Cell Biol.* **2015**, *210*, 883–890. [[CrossRef](#)] [[PubMed](#)]
40. Csordas, G.; Weaver, D.; Hajnoczky, G. Endoplasmic Reticulum-Mitochondrial Contactology: Structure and Signaling Functions. *Trends Cell Biol.* **2018**, *28*, 523–540. [[CrossRef](#)] [[PubMed](#)]
41. Kornmann, B.; Currie, E.; Collins, S.R.; Schuldiner, M.; Nunnari, J.; Weissman, J.S.; Walter, P. An ER-mitochondria tethering complex revealed by a synthetic biology screen. *Science* **2009**, *325*, 477–481. [[CrossRef](#)] [[PubMed](#)]
42. Koch, K.V.; Suelmann, R.; Fischer, R. Deletion of mdmB impairs mitochondrial distribution and morphology in *Aspergillus nidulans*. *Cell Motil. Cytoskelet.* **2003**, *55*, 114–124. [[CrossRef](#)]
43. Lee, H.; Yoon, Y. Transient Contraction of Mitochondria Induces Depolarization through the Inner Membrane Dynamin OPA1 Protein. *J. Biol. Chem.* **2014**, *289*, 11862–11872. [[CrossRef](#)]
44. Wolf, D.M.; Segawa, M.; Kondadi, A.K.; Anand, R.; Bailey, S.T.; Reichert, A.S.; van der Blik, A.M.; Shackelford, D.B.; Liesa, M.; Shirihai, O.S. Individual cristae within the same mitochondrion display different membrane potentials and are functionally independent. *Embo. J.* **2019**, *38*, e101056. [[CrossRef](#)] [[PubMed](#)]
45. Cho, B.; Cho, H.M.; Jo, Y.; Kim, H.D.; Song, M.; Moon, C.; Kim, H.; Kim, K.; Sesaki, H.; Rhyu, I.J.; et al. Constriction of the mitochondrial inner compartment is a priming event for mitochondrial division. *Nat. Commun.* **2017**, *8*, 15754. [[CrossRef](#)] [[PubMed](#)]
46. Hernández-Becerril, A. Evaluación de NoxR y RacA Como Posibles Reguladores de la Actividad de NADPH Oxidasa NoxA de *Aspergillus nidulans*. Masters degree Thesis, Universidad Nacional Autónoma de México, México city, Mexico, 2010.
47. Geissel, B.; Penka, M.; Neubauer, M.; Wagener, J. The ER-mitochondria encounter structure contributes to hyphal growth, mitochondrial morphology and virulence of the pathogenic mold *Aspergillus fumigatus*. *Int. J. Med. Microbiol.* **2017**, *307*, 37–43. [[CrossRef](#)] [[PubMed](#)]
48. Lang, A.; Peter, A.T.J.; Kornmann, B. ER-mitochondria contact sites in yeast: Beyond the myths of ERMES. *Curr. Opin. Cell Biol.* **2015**, *35*, 7–12. [[CrossRef](#)]
49. Debattisti, V.; Gerencser, A.A.; Saotome, M.; Das, S.; Hajnoczky, G. ROS Control Mitochondrial Motility through p38 and the Motor Adaptor Miro/Trak. *Cell Rep.* **2017**, *21*, 1667–1680. [[CrossRef](#)]
50. Hung, C.H.L.; Cheng, S.S.Y.; Cheung, Y.T.; Wuwongse, S.; Zhang, N.Q.; Ho, Y.S.; Lee, S.M.Y.; Chang, R.C.C. A reciprocal relationship between reactive oxygen species and mitochondrial dynamics in neurodegeneration. *Redox. Biol.* **2018**, *14*, 7–19. [[CrossRef](#)] [[PubMed](#)]
51. Miyazono, Y.; Hirashima, S.; Ishihara, N.; Kusukawa, J.; Nakamura, K.; Ohta, K. Uncoupled mitochondria quickly shorten along their long axis to form indented spheroids, instead of rings, in a fission-independent manner. *Sci. Rep.* **2018**, *8*, 350. [[CrossRef](#)]
52. Aklima, J.; Onojima, T.; Kimura, S.; Umiuchi, K.; Shibata, T.; Kuraoka, Y.; Oie, Y.; Sukanuma, Y.; Ohta, Y. Effects of Matrix pH on Spontaneous Transient Depolarization and Reactive Oxygen Species Production in Mitochondria. *Front. Cell Dev. Biol.* **2021**, *9*, 1582. [[CrossRef](#)] [[PubMed](#)]
53. Bonora, M.; Giorgi, C.; Pinton, P. Molecular mechanisms and consequences of mitochondrial permeability transition. *Nat. Rev. Mol. Cell Bio* **2022**, *23*, 266–285. [[CrossRef](#)]
54. Booth, D.M.; Varnai, P.; Joseph, S.K.; Hajnoczky, G. Oxidative bursts of single mitochondria mediate retrograde signaling toward the ER. *Mol. Cell* **2021**, *81*, 3866–3876.e2. [[CrossRef](#)] [[PubMed](#)]

55. Fung, T.S.; Chakrabarti, R.; Kollasser, J.; Rottner, K.; Stradal, T.E.B.; Kage, F.; Higgs, H.N. Parallel kinase pathways stimulate actin polymerization at depolarized mitochondria. *Curr. Biol.* **2022**, *32*, 1577–1592.e8. [[CrossRef](#)] [[PubMed](#)]
56. Mattie, S.; Krols, M.; McBride, H.M. The enigma of an interconnected mitochondrial reticulum: New insights into mitochondrial fusion. *Curr. Opin. Cell Biol.* **2019**, *59*, 159–166. [[CrossRef](#)] [[PubMed](#)]
57. Mottie, S.; Riemer, J.; Wideman, J.G.; McBride, H.M. A new mitofusin topology places the redox-regulated C terminus in the mitochondrial intermembrane space. *J. Cell Biol.* **2018**, *217*, 507–515. [[CrossRef](#)]
58. Shutt, T.; Geoffrion, M.; Milne, R.; McBride, H.M. The intracellular redox state is a core determinant of mitochondrial fusion. *Embo. Rep.* **2012**, *13*, 909–915. [[CrossRef](#)]
59. Kuroiwa, T.; Nishida, K.; Yoshida, Y.; Fujiwara, T.; Mori, T.; Kuroiwa, H.; Misumi, O. Structure, function and evolution of the mitochondrial division apparatus. *BBA Mol. Cell Res.* **2006**, *1763*, 510–521. [[CrossRef](#)]